Molecular dynamics method to locally resolve Poisson's ratio: Mechanical description of the solid–soft-matter interphase

Enrico Riccardi,* Michael C. Böhm, and Florian Müller-Plathe
Eduard-Zintl-Institut für Anorganische und Physikalische Chemie, Technische Universität Darmstadt, Petersenstrasse 20, D-64287 Darmstadt, Germany
(Received 22 May 2012; published 27 September 2012)

A method based on "small-deformation mechanical response" has been developed to locally resolve the Poisson's ratio via molecular dynamics simulations. The approach can be used for simple and composite materials to characterize systems with two or more continuous phases in the framework of periodic boundary conditions. The proposed technique represents a simple method to obtain a local mechanical description of complex systems. A polystyrene bulk, a silica bulk, and a polystyrene-silica heterogeneous composite material have been characterized under imposed strain. The results show the effects of local material inhomogeneities which are present in the glassy material and in the composite system. The Poisson's ratio spatial profiles for silica, the polystyrene bulk, and in the interphase region between the soft polymer bulk and the hard surface have also been calculated. The obtained local mechanical description can be employed in micromechanical models developed to predict the overall mechanical properties of multicomponent materials.

DOI: 10.1103/PhysRevE.86.036704 PACS number(s): 05.10.−a, 62.20.F−, 62.25.−g, 46.15.−x

I. INTRODUCTION

The mechanical modeling of a material requires the determination of relationships between the imposed stresses and the induced strains and vice versa. These relations are defined as constitutive equations and allow the description and prediction of mechanical material properties. With the development of new complex materials, such as nanocomposites [1], refined models are demanded in engineering applications to describe the influences of mechanical stress [2]. Nanocomposites are complex multicomponent multiphase materials and, generally, are formed by a polymer matrix in which nanofillers with dimensions of a few nanometers are dispersed [3–5]. The main reason for the interest in these materials is their highly customizable properties [6] which can be tuned, in principle, by varying the constituents' characteristics and their composition ratios. Consequently, researchers' efforts have been directed towards the development of models able to describe the mechanical properties of nanocomposite materials. The need for further model enhancements to predict the mechanical behavior of these complex materials with sufficient accuracy has been reported widely [7–10].

When at least one of the nanomaterial constituents is composed of soft matter, the interactions between the constituents modify the soft material microstructure in the interphase layer [5,11]. It is therefore of interest to develop models able to map possible changes in the interphase layer in order to predict the mechanical properties of such composite materials. Several studies have shown that the overall characteristics of nanocomposites can deviate significantly from simplistic expectations based on a component characteristic sum or average [12]. As a result, numerical studies have been performed in the attempt to develop new micromechanical models to account for the properties of the individual constituents and of the interphase regions of nanocomposites [13,14]. Generally, multiscale models are one of the most efficient approaches to describe and predict the properties of nanocomposite materials [15] since low-resolution descriptions of bulk regions can be merged with high-resolution descriptions in the interfacial regions, thus optimizing the computational effort. Depending on the desired level of resolution and on the size of the interfacial regions, two main multiscale approaches can be employed: (i) the direct and iterative strain-stress exchange between the molecular simulation domain and the upscale domain, e.g., by the finite-element method [16,17]. and (ii) the determination of locally resolved elastic coefficients required to solve the constitutive equations of micromechanical models in each phase and in the interfacial region. Molecular simulations can provide spatially resolved mechanical quantities as a function of the distance from an interface [18]. By means of an equivalent-continuum model [19] or through a "homogenization" procedure [20]. locally resolved elastic coefficients can be implemented in a micromechanical model to study the overall material behavior. Approach (i) is, in principle, more accurate than approach (ii), at the cost of greater computational requirements, while approach (ii) requires the study and the mechanical analysis of only a single system. Within approach (ii), a composite material constituted by a soft phase in the presence of nanofillers has been studied and its overall mechanical properties have been described [18,20].

The methods used to compute elastic coefficients via molecular simulations can be divided into three branches [21]: (a) "fluctuation methods" based on linear response theory and the theory of elasticity, where thermal averages of strain or stress fluctuations are considered [22–27], (b) "dynamic methods," in which the stress-strain correlation in a material can be computed from constant stress simulations [28–32], and (c) "small-deformation mechanical response" approaches, in which the strain is imposed by position rescaling followed by an energy minimization procedure, after which the system's response is computed [33,34]. In principle, fluctuation methods are preferable as they require only a single equilibrium

*Author to whom correspondence should be addressed: e.riccardi82@gmail.com

simulation from which the compliance tensor of a material can be computed, thus completely defining the mechanical properties of a system in the elastic regime. In glassy polymers, fluctuation methods suffer from convergence limitations that hinder their application. If, in addition, a local resolution of mechanical quantities is intended, the results obtained would not be reliable. Herein, for a glassy polymer, methods (b) and (c) seem the most reliable approaches. Since the focus of the present work is the development of a technique to locally describe the mechanical properties of a multicomponent system, a mechanical descriptor and a method only moderately affected by statistical fluctuations have been selected and designed. To resolve the Poisson's ratio locally, the local displacement profile induced by an imposed strain or stress is the only quantity needed. As reported by Greaves *et al.*, "In comparing a material's resistance to distort under mechanical load rather than to alter in volume, Poisson's ratio offers the fundamental metric by which to compare the performance of any material when strained elastically" [35]. In comparison to other mechanical coefficients which require the computation of local pressures, such as the Young's modulus, the Poisson's ratio is expected to be influenced less by statistical fluctuations. Therefore, the locally resolved Poisson's ratio renders possible a simple and efficient mechanical description.

In the present work, a method based on the small-deformation mechanical response approach, i.e., method (c), has been developed to locally compute the Poisson's ratio via molecular dynamics (MD) simulations. For the computation of the mechanical response of a system on which a stress or a strain is imposed, the implementation of boundary conditions has to be consistent with the imposed stress-strain scheme. Boundary conditions with flexible simulation boxes, such as the "elastic minimum image convention" method [36] or stochastic boundary conditions [16], represent acceptable candidates that allow the computation of locally resolved elastic coefficients. However, the complexity of such a method implementation would increase significantly without leading to concrete benefits in the present framework. The commonly applied periodic boundary conditions (PBCs) have the drawback of preserving the shape of the simulation box. Therefore, the imposition of a uniaxial and uniform stress or strain, as in method (b), would induce local displacements that are a function of the overall material properties, thus neglecting local effects. PBCs, however, can be employed only if by imposing a stress or strain along two directions uniformly local contributions from the third direction are obtained independently. As such, a generalization of the Poisson's ratio definition is proposed in the present work that is consistent with periodic boundary conditions, thus enabling a simple implementation in molecular simulation techniques.

The approach presented herein to compute the spatial profile of the Poisson's ratio is of sufficient generality to allow the characterization of systems in which the constituents have different mechanical properties (e.g., crystals and glassy polymers), with a special focus on the characterization of the interphase region. A polystyrene bulk, a silica bulk, and a polystyrene-silica composite system separated by a flat interface have then been described with the developed technique. The derived spatial profile of the Poisson's ratio can be implemented directly in a micromechanical model for different types, sizes, and shapes of nanofiller inclusions by employing a "homogenization" procedure [20]. The flat interface considered in the present work allows the evaluation of the Poisson's ratio in the interphase around nanofillers whose dimensions are large enough to neglect the effects of the surface curvature on the mechanical property spatial profiles.

II. METHOD AND MODELS

The definition of the Poisson's ratio for the conventional strain scheme depicted in Fig. 1(a) is

$$\nu = -\frac{\varepsilon_{\text{induced}}}{\varepsilon_{\text{imposed}}}, \tag{1}$$

where $\varepsilon_{\text{imposed}}$ is the axial strain in the direction of the imposed deformation and $\varepsilon_{\text{induced}}$ the induced strain measured along one of the directions orthogonal to the vector of the imposed strain. Equation (1) assumes that the imposed strain is along only one direction and that the induced strain appears in the plane normal to the imposed strain, as schematically depicted in Fig. 1(a). In a multiphase system, in which a continuous phase is present, limitations in the imposition of the external strain or stress are introduced due to PBCs. For instance, assuming that the interface region extends along the x and y directions and applying a compression along the z axis, the resulting lateral expansion along the x and y axes will be determined by the stiffest phase of the composite system. As a consequence, the induced lateral displacements in a multiphase material with different mechanical properties cannot be calculated independently in a MD simulation with PBCs. Therefore, the imposed or induced strain scheme in Fig. 1(a) is not applicable.

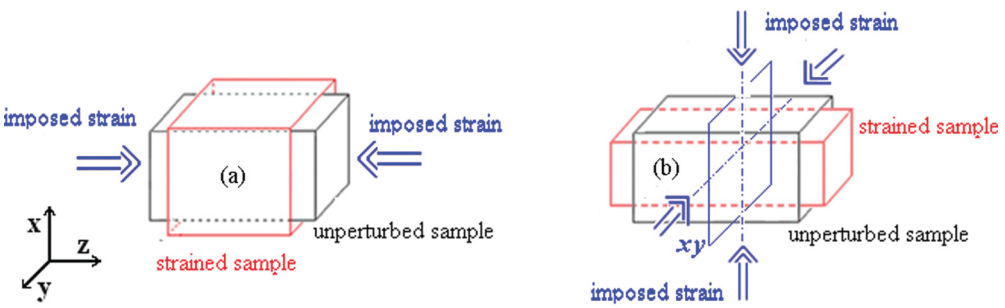

FIG. 1. (Color online) Schematic representation of the imposed/induced strain in a general test sample. (a) The commonly used imposed-induced displacement convention to compute the Poisson's ratio. (b) The displacement scheme consistent with PBCs.

If, instead, a uniform compression or expansion is imposed along the two axes defining the plane parallel to the surface, a strain along the normal direction to the plane will be induced, as depicted in Fig. 1(b). Adopting this strategy, each phase in the system will be able to relax almost independently under consideration of PBCs. Therefore, the overall system compression or expansion along the axis normal to the surface can be expressed as the sum of local deformations. In the present work, the strain will be imposed consistently along the xy plane, while the Poisson's ratio will be mapped along the z direction normal to the xy plane.

For the strain scheme represented in Fig. 1(b), a reformulation of a mechanical quantity such as the Poisson's ratio is necessary. The matrix of the elastic stiffness coefficients, $\bar{\bar{C}}$, relates strain ($\bar{\varepsilon}$) and stress ($\bar{\sigma}$),

$$\bar{\sigma} = \bar{\bar{C}}\bar{\varepsilon} \tag{2}$$

and, for isotropic and linear elastic materials,

$$\begin{bmatrix} \sigma_{xx} \\ \sigma_{yy} \\ \sigma_{zz} \\ \sigma_{yz} \\ \sigma_{xy} \\ \sigma_{xz} \end{bmatrix} = \frac{1}{E} \begin{bmatrix} 1 & -\nu & -\nu & 0 & 0 & 0 \\ -\nu & 1 & -\nu & 0 & 0 & 0 \\ -\nu & -\nu & 1 & 0 & 0 & 0 \\ 0 & 0 & 0 & 2(1+\nu) & 0 & 0 \\ 0 & 0 & 0 & 0 & 2(1+\nu) & 0 \\ 0 & 0 & 0 & 0 & 0 & 2(1+\nu) \end{bmatrix} \begin{bmatrix} \varepsilon_{xx} \\ \varepsilon_{yy} \\ \varepsilon_{zz} \\ \varepsilon_{yz} \\ \varepsilon_{xy} \\ \varepsilon_{xz} \end{bmatrix}, \tag{3}$$

where E is the Young modulus; σ_{ij} and ε_{ij} are the elements of the symmetrical tensors of stress, $\bar{\sigma}$, and of strain, $\bar{\varepsilon}$, rearranged as vectors. For the strain scheme shown in Fig. 1(b), $\sigma_{yz} = \sigma_{xy} = \sigma_{xz} = 0$, $\varepsilon_{xx} = \varepsilon_{yy} = \varepsilon_{\parallel}$, and $\sigma_{xx} = \sigma_{yy} = \sigma_{\parallel}$ can be defined. In mechanical equilibrium, the stress σ_{zz} is equal to 0, therefore Eq. (3) results in a set of two linear equations,

$$\sigma_{\parallel} - \nu\sigma_{\parallel} = E\varepsilon_{\parallel}, \tag{4a}$$

$$-2\nu\sigma_{\parallel} = E\varepsilon_{zz}, \tag{4b}$$

that can be satisfied simultaneously with

$$\nu = -\frac{\varepsilon_{zz}}{2\varepsilon_{\parallel} - \varepsilon_{zz}}. \tag{5}$$

The reformulation of the Poisson's ratio obtained here, besides allowing the application of a strain scheme compatible with PBCs, is also consistent with the limiting cases of an incompressible material ($\nu = 0.5$), as well as materials that do not show normal strain as response to an imposed strain ($\nu = 0$).

In the present work, the imposed biaxial strain has been applied through atomic positions and box dimensions rescaling (Fig. 2, step 1),

$$r'_{x,i} = \alpha r_{x,i},\ r'_{y,i} = \beta r_{y,i},\ r'_{z,i} = \gamma r_{z,i},\ i = 1, \ldots, N_p^{\text{tot}} \tag{6a}$$

and

$$L'_x = \alpha L_x,\ L'_y = \beta L_y,\ L'_z = \gamma L_z, \tag{6b}$$

where N_p^{tot} is the total particle number in the system, $r_{k,i}$ is the k component ($k = x, y, z$) of the initial position vector, $\bar{r}_i$, of particle i; $r'_{k,i}$ is the k component of the rescaled position vector, $\bar{r}'_i$, of particle i. L_k is the initial overall box dimension along the k direction, and L'_k is the rescaled overall box dimension along the k direction. α, β, and γ are the position rescaling factors along the x, y, and z axes, respectively. Assuming $\alpha = \beta$, a uniform biaxial strain is imposed along the x and y directions (for a 3% biaxial compression, $\alpha = \beta = 0.97$, $\gamma = 1$). The obtained coordinate vectors, $\vec{r}'_i$ for $i = 1, \ldots, N_p^{\text{tot}}$ describe the rescaled system configuration, which has to be reequilibrated keeping the x and y simulation box dimensions, L'_x and L'_y, constant (Fig. 2, step 2), thus simulating a constant imposed strain. A scheme of the adopted strategy is shown in Fig. 2. (The Cartesian axes convention in the present work is consistent with the axes convention shown in Figs. 1 and 2).

The spatial profile of the Poisson's ratio along the axis normal to a plane, here the z axis, can be computed from the normal local atomic displacements induced by the strains imposed parallel to that plane, here the x and y directions. In the framework of MD, the atomic displacement profile along any direction can be evaluated as

$$dr_{k,i} = \langle r''_{k,i} \rangle - \langle r_{k,i} \rangle \quad \text{for } k = x, y, z, \tag{7}$$

where $dr_{k,i}$ is the average displacement of particle i in the direction of the k axis, $\langle r_{k,i} \rangle$ the average component of the position vector, $\bar{r}_i$, of particle i with respect to the k axis in the equilibrated unperturbed state [Fig. 2(a)], while $\langle r''_{k,i} \rangle$ is the average atomic position of particle i along the k axis in the strained reequilibrated system [Fig. 2(c)]. Two different simulation sets are therefore necessary to compute the averaged $\langle r_{k,i} \rangle$ and $\langle r''_{k,i} \rangle$. The $\langle r_{k,i} \rangle$ can be calculated from the equilibrated unperturbed system, while $\langle r''_{k,i} \rangle$ can be obtained from a reequilibrated system in which the imposed strain is maintained. Once $\langle r_{k,i} \rangle$ and $\langle r''_{k,i} \rangle$ have been determined, it is possible to measure the local deformations induced by the imposed displacements. It should be noted that $\langle r_{k,i} \rangle$ can be computed only for nondiffusive systems, such as a solid or a glass.

The spatial distribution of the atomic displacements along the z axis renders possible the local resolution of the Poisson's ratio. In order to reduce the noise in the local values of the elastic coefficient, the atomic displacement has to be averaged locally. It is therefore convenient to adopt a volume averaging criterion, subdividing the system into fictitious slabs with a constant number of particles, N_{ps}. Once N_{ps} has been selected,

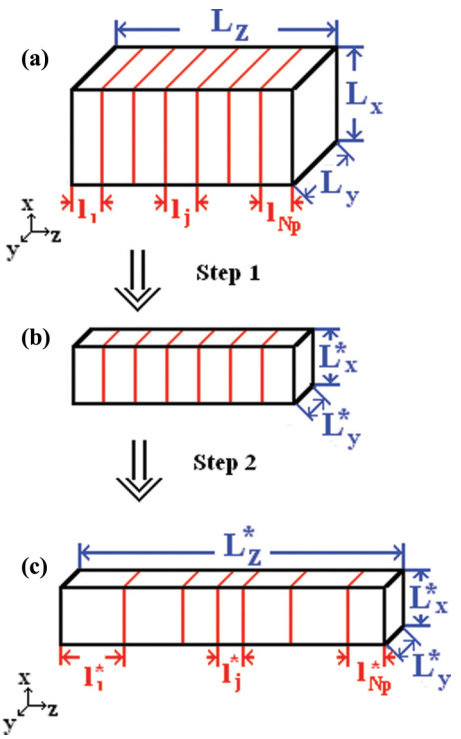

FIG. 2. (Color online) Schematic representation of the strategy to locally resolve the Poisson's ratio: (a) Equilibrated unperturbed system, (b) atomic position rescaling along the x and y axes. A predetermined strain is imposed along the x and y directions. (c) Reequilibration step with the system dimensions x and y fixed. In the figure, L_k for $k = x, y, z$ is the initial overall box dimension along the x, y, z directions, L'_k for $k = x, y, z$ is the rescaled box dimension, and L''_k for $k = x, y, z$ the final, i.e., relaxed overall simulation box dimension, $L'_x = \alpha L_x$ and $L'_y = \beta L_y$, where α and β are the position rescaling factors for the x and y directions, respectively, $L'_x = L''_x$ and $L'_y = L''_y$. l_j is the initial dimension of slab j in the z direction, L''_j is the final dimension of slab j in the z direction, and N_{sl} is the total number of slabs. For $\gamma = 1$ the rescaled slab length, l'_j, is equal to l_j and $L_z = L'_z$.

setting the particle index label according to the z position of the particle such as $\langle r_{z,i}\rangle > \langle r_{z,i-1}\rangle$ for $i = 2, \ldots, N_p^{\text{tot}}$, the length of the jth slab, l_j, can be readily computed:

$$\begin{aligned} l_j &= \langle r_{z,a}\rangle - \langle r_{z,b}\rangle, \quad a = jN_{ps}, \\ b &= (j-1)N_{ps} + 1, \quad j = 1, \ldots, N_{sl}, \end{aligned} \tag{8}$$

where N_{sl} is the total number of slabs. Once the strain has been imposed and the system reequilibrated, resetting the particle index according to the new particle position in the strained system such as $r''_{z,i} > r''_{z,i-1}$, the new slab dimensions can be readily computed:

$$\begin{aligned} l''_j &= \langle r''_{z,a}\rangle - \langle r''_{z,b}\rangle, \quad a = jN_{ps}, \\ b &= (j-1)N_{ps} + 1, \quad j = 1, \ldots, N_{sl}. \end{aligned} \tag{9}$$

From the global and locally induced strain, the overall average value of the Poisson's ratio, ν_{system}, and the local value in each slab thus can be computed. ν_{system} can be determined according to Eq. (5):

$$\nu_{\text{system}} = -\frac{\frac{(L''_z - L_z)}{L_z}}{2\frac{(L''_x - L_x)}{L_x} - \frac{(L''_z - L_z)}{L_z}} = -\frac{\frac{(L''_z - L_z)}{L_z}}{2\frac{(L''_y - L_y)}{L_y} - \frac{(L''_z - L_z)}{L_z}}. \tag{10}$$

Under the assumption that the induced local strains are independent from each other, the locally resolved Poisson's ratio, ν_j, for slab j can be obtained from

$$\begin{aligned} \nu_j &= -\frac{\frac{(l''_j - l_j)}{l_j}}{2\frac{(L''_x - L_x)}{L_x} - \frac{(l''_j - l_j)}{l_j}} = -\frac{\frac{(l''_j - l_j)}{l_j}}{2\frac{(L''_y - L_y)}{L_y} - \frac{(l''_j - l_j)}{l_j}}, \\ j &= 1, \ldots, N_{sl}. \end{aligned} \tag{11}$$

Under the assumption $L_z \cong \sum_{j=1}^{N_{sl}} l_j$ and $L''_z \cong \sum_{j=1}^{N_{sl}} l''_j$, and, following an averaging criterion for parallel springs, one can obtain

$$\nu_{\text{system}} \cong \frac{1}{N_{sl}} \sum_{j=1}^{N_{sl}} \nu_j. \tag{12}$$

The selection of the particle numbers or, equivalently, the average dimension of each slab influences the resolution of the method and the magnitude of the statistical fluctuations. The standard deviation for the locally resolved elastic quantity can be also computed:

$$\text{stdev} = \sqrt{\sum_{j=1}^{N_{sl}} \frac{(\nu_{\text{system}} - \nu_j)^2}{N_{sl}}}. \tag{13}$$

It should be noted that Eq. (13) can be applied directly only when the overall ν_{system} and the local values, ν_j, of the Poisson's ratio refer to the same material. Thermal fluctuations and material inhomogeneities generate a certain noise in the profile of the induced atomic displacements and, therefore, in the accessible local resolution in the spatial profile of the Poisson's ratio. Any enhancement in the local resolution, i.e., increased number of slabs, is accompanied by an increasing statistical noise. Therefore, in order to estimate the accessible local resolution in an inhomogeneous system, the computational error has to be determined as a function of the averaging volume. Once the volume required to obtain a local resolution within a certain accuracy has been determined in a reference bulk system, the study of surface effects on the spatial profile of the Poisson's ratio in the soft-matter phase becomes possible. It is worth to emphasize that the spatial profile of the elastic quantity has been approximated as a sequence of adjacent homogeneous and isotropic subsystems. Even if the Poisson's ratio can be defined for both isotropic and anisotropic systems [37], for simplicity and for geometrical limitations of the interfacial system, an average Poisson's ratio under the assumption of an isotropic system has been computed. This assumption is suitable for amorphous media, while it only allows the discrimination between a *nonauxetic* and *effectively auxetic* [37] behavior in a structurated material with directional properties.

In the present work, molecular simulations have been performed using MD. The unperturbed systems have been simulated for a constant number of particles, pressure, and temperature (*NPT* ensemble). Thereafter, in the strained systems,

the imposed deformation along the x and y axes has been kept constant, fixing the lateral dimensions of the cross-sectional area A_{xy}, while relaxation along the direction normal to the imposed biaxial strains, z, has been allowed by controlling only the pressure component, P_z ($NA_{x,y}\mathrm{P}_z T$ ensemble).

III. MODELS AND SIMULATION DETAILS

Molecular dynamics simulations have been performed to calculate the Poisson's ratios of an atactic polystyrene (PS) bulk, an α-quartz silica (SiO_2) bulk, and an interfacial composite of atactic PS in contact with a flat silica surface. The PS chains ($-[C_8H_8]_{20}-$) have been terminated by a methyl group (-CH_3), while periodic boundary conditions along the three directions have been applied for the silica bulk. The surface silica oxygen atoms in the composite system were saturated with hydrogen atoms.

An in-house developed MD simulation code, YASP [38], was used to simulate the polymer PS and α-quartz silica with full atomic resolution. The force-field parameters for PS are based on the OPLS-AA method [39] for hydrocarbon systems which has been optimized to describe mixtures of PS with benzene [40] and ethylbenzene [41]. In this force field, the carbon and hydrogen atoms of the phenyl rings have partial charges to reproduce the electric quadrupole moment, while harmonic dihedral angles were employed in the phenyl rings to maintain planarity. The interaction parameters within the silica phase have been obtained from a crystalline silica bulk model [42], in which silica and oxygen atoms carry partial charges, too. On the silica surface, the hydrogens carry a partial positive charge, allowing electroneutrality in the overall silica phase. Within the silica phase, two-body interactions and a bending potential between three consecutive atoms are considered. The intermolecular interactions have been modeled with Lennard-Jones (LJ) and Coulomb potentials using Lorentz-Berthelot mixing rules [43]. The Kirkwood approximation in the reaction-field method [44] has been used to correct the interaction potential beyond the cutoff distance, taken equal to 1.0 nm. An effective relative permittivity of the continuum $\varepsilon_{\mathrm{RF}}$ of 3.7 (experimental relative permittivities: 2.4–2.7 for amorphous PS and 4.4–4.6 for amorphous silica at room temperature) [45] has been chosen. A complete description of the force field employed for the intra- and intermolecular interactions of polystyrene and silica can be found in the work of Ndoro *et al.* [5]. The silica model adopted here mimics the crystalline silica structure but generates a known density offset [5,46,47]. It has been kept in the present work for consistency with our previous investigations [5,46,47] and since the main focus of the present work concerns the study of interfacial effects in the soft-matter phase.

System (a) is a polymeric bulk composed of 200 polystyrene chains, 20 monomers long, for a total of 64 400 atoms in a simulation box with dimensions 8.7 × 8.8 × 8.7 nm in the unperturbed state. System (b1) is a SiO_2 bulk formed of 17 280 atoms in a simulation box with dimensions 6.3 × 5.7 × 7.2 nm in the unperturbed state. A silica wafer, system (b2), with dimensions 9.4 × 9.2 × 2.5 nm for a total of 15 120 atoms in six atomic layers has been also constructed. The composite system, here labeled as system (c), has been built by combining systems (a) and (b2) for a total of 79 520 atoms in a box with overall dimensions of 9.4 × 9.2 × 9.9 nm in the unperturbed state. For all systems considered, periodic boundary conditions have been imposed along all directions.

Polystyrene is an amorphous polymeric material. Its simulation requires efficient equilibration procedures in order to obtain initial configurations with only moderate finite-size effects and metastabilities in acceptable times [48]. To study the atactic polystyrene system (a), a set of ten independent simulations with identical particle numbers and simulation conditions but independent initial configurations have been generated. In each system, 200 polymeric chains 20 monomers long with random initial positions and orientations have been introduced and equilibrated in coarse-grained (CG) resolution for 10 ns at 300 K and 101.3 kPa in the *NPT* ensemble. The CG model adopted for PS has been developed via the pressure-corrected iterative Boltzmann inversion method [49] and it models each polystyrene monomer by one coarse-grained bead. The obtained coarse-grained configuration has then been back-mapped, providing a full atomistic description of the system. A complete description of the CG simulation details can be found in the work of Qian *et al.* [41], while the description of the topologically guided back-mapping procedure adopted can be found in the work of Ghanbari *et al.* [50] The obtained configurations for the ten systems with independent initial conditions simulated in full atomistic detail have been further equilibrated for additional 10 ns in the *NPT* ensemble. The average density of the simulated PS systems is equal to 1033.9 kg/m^3, while the total energy of the PS systems amounts to 390.865 MJ/mol with a variation coefficient of 0.097%. The values of the density and of the total system energy recorded every 1 ps for a time span of 1 ns have linear regression coefficients equal to 0.065 and 0.289, respectively. The density value recorded in the simulations is in good agreement with the value of 1045 kg/m^3 measured experimentally [51].

The silica bulk, system (b1), and the silica wafer, system (b2), have been constructed in accordance with the α-quartz crystalline structure [42] for consistency with our previous investigations [5,46,47]. The unit cells of the silica wafer have been oriented such that the external surfaces correspond to the crystallographic 1-0-0 plane. A simulation of 0.1 ns has been sufficient to reach equilibration. The adopted force field describes correctly the α-quartz structure but underestimates the material density. The density of the simulated silica bulk and of the silica wafer is equal to 2193.5 kg/m^3, with 0.05% variation coefficient, while a density of 2647 kg/m^3, with 1.5% variation coefficient, has been measured experimentally [52–54].

The polystyrene-silica composite systems have been constructed by positioning the wafer of silica, system (b2), in the equilibrated polystyrene bulk. To allow the insertion of the wafer, the PBCs into the direction normal to the surface have been removed temporarily. Then the silica phase has been added, avoiding overlaps with the polymeric chains. By reintroducing PBCs along every direction, a temperature annealing procedure at 600 K has been performed. The composite system has been kept for 10 ns at 600 K and then cooled down with a cooling rate of -50 K/ns. Once the desired temperature of 300 K has been reached, the composite systems have been run for a further 5 ns. The overall composite density computed in the simulations is 1231.0 kg/m^3 with a

variation coefficient of 0.075%, while the total energy was 2113.8 MJ/mol with a variation coefficient of 0.05%. The values of the density and total system energy have been recorded every 1 ps for a time span of 1 ns and their values as a function of time have linear regression coefficients equal to 0.004 78 and -0.066, respectively.

Once the systems have been equilibrated, the production runs for the unperturbed samples have been performed at constant temperature T and pressure P, employing Berendsen's thermostat weak coupling [55] to a temperature bath of 300 K and a pressure bath of 101.3 kPa. The coupling times were 0.2 (T) and 0.5 ps (P), where a time step of 1 fs was employed. For the strained system, a constant temperature T, constant normal pressure to the xy surface P_z, and a constant cross sectional area A (xy) have been assumed (NP_zAT ensemble). The results reported for the atomic displacements and Poisson's ratio profiles have been obtained from a time average over 1000 frames output at 1 ns intervals.

IV. RESULTS AND DISCUSSION

The developed method has been adopted first for the polymer bulk reference system (a). Biaxial strains have been applied along two axes, x and y, and the induced atomic displacements along the x, y, and z axes have been measured according to Eq. (7). The magnitude of the imposed biaxial strain, which has to occur in the elastic strain range of polystyrene, should be a compromise between (i) the time interval required to reequilibrate a higher strained system and (ii) the relative amplitude of the statistical fluctuations in the computed atomic displacements. Different magnitudes of the biaxial compression and expansion within the elastic regime have been imposed in several independent simulations. A value of 3% appeared to be an acceptable compromise between (i) and (ii) and thus has been selected for further analysis. The induced atomic displacements in the x, y, and z directions for the bulk system (a) have been plotted as a function of the z coordinate in Figs. 3(a) and 3(b) for a 3% biaxial compression, and in Figs. 3(c) and 3(d) for a 3% biaxial expansion. In Fig. 3, and in Fig. 8 to be discussed later, the atomic displacement profiles, dr_k for $k = x,y,z$, are obtained from the local averages of the atomic displacements $dr_{x,i}$ per slab, for $k = x$, y, z, respectively, while dR_k, for $k = x,y,z$, refers to the atomic displacements in the frame of reference of the homogeneous linear displacement ($dR_x = dr_x$, $dR_y = dr_y$, and $dR_Z = dr_z - (Az - B)$ where A and B are the coefficients computed from the linear regression of the dr_z spatial profile).

With the exception of some foams and structured materials [37,52], which have a negative Poisson's ratio, a

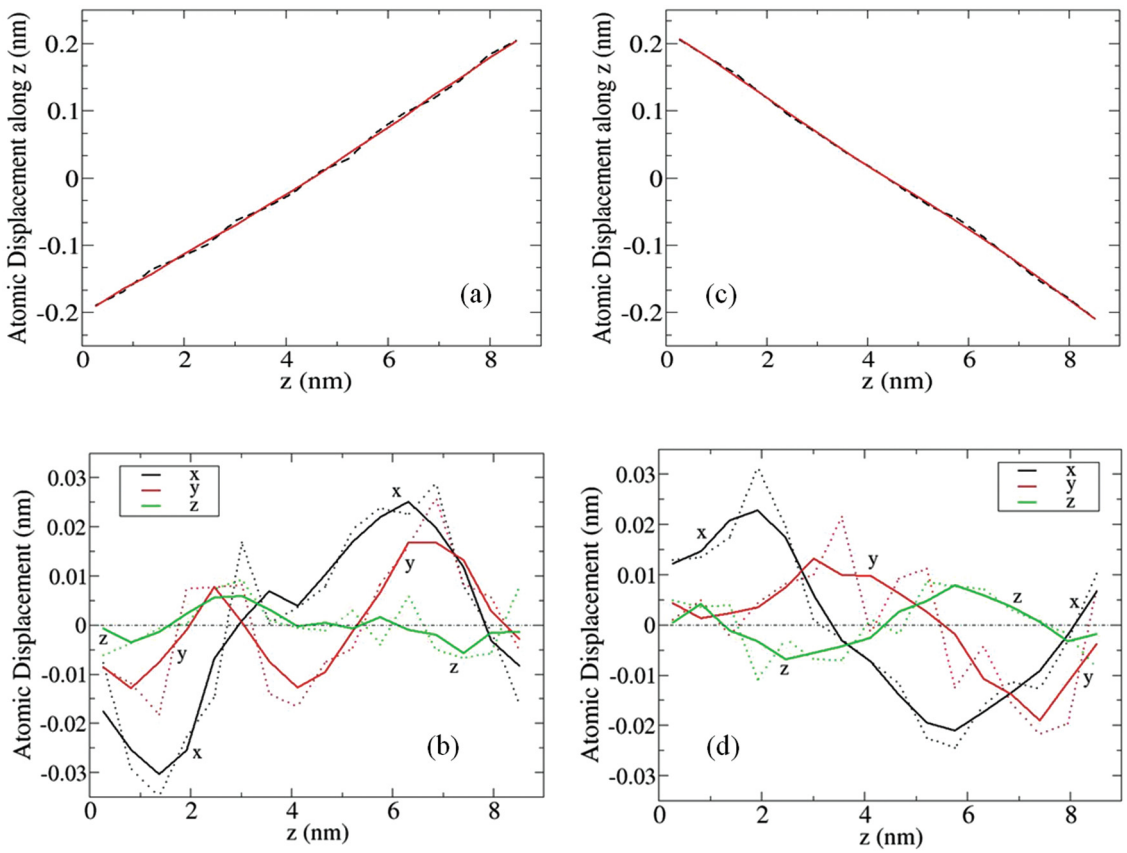

FIG. 3. (Color online) Local atomic displacement for the polystyrene bulk system under 3% imposed biaxial strain. Plots (a) and (c) show the local atomic displacement dR_z profiles as a function of the z coordinate for the biaxial compression and expansion test, respectively. The spatial profile of the induced atomic displacements dR_x, dR_y, dR_z is reported in plot (b) for the compression test and in plot (d) for the expansion test in the frame of reference of the average linear displacement. In the plots, the dotted profiles represent the local displacement values, while the continuous profiles report the five point running average of the atomic displacement profile.

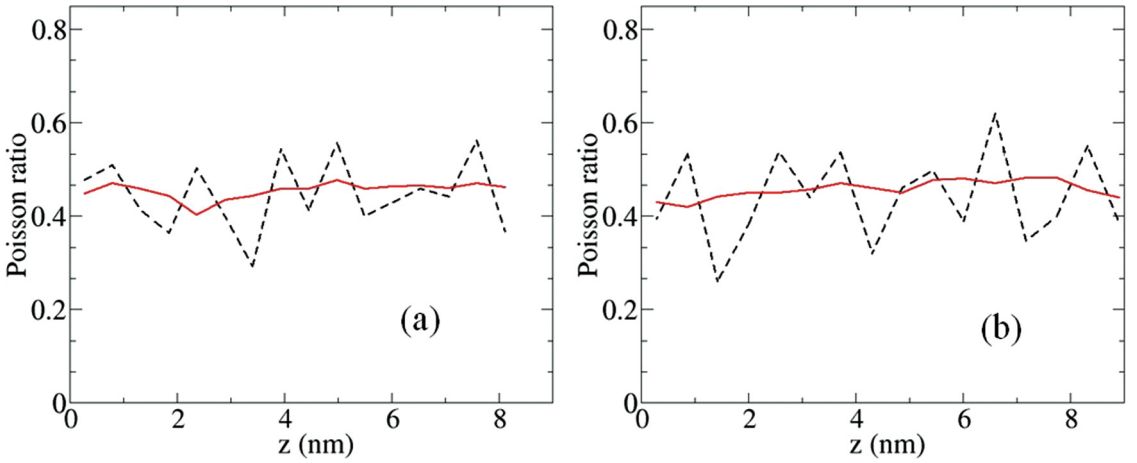

FIG. 4. (Color online) Local Poisson's ratio for a PS bulk under 3% biaxial compression (a) and expansion (b). In the plots, the dashed black profile reports the local Poisson's ratio values, while the continuous red profile reports the running average of the Poisson's ratio spatial profile.

compression along one axis generates an expansion into the other direction(s). Applying a compression along the x and y axes, an expansion along the z axis will thereby be generated. Consistently, Fig. 3(a) shows that the PS bulk system elongates in the z direction and the slope of the computed atomic displacements is positive. In the case of a biaxial expansion a system compression in the z direction is measured instead, as shown in Fig. 3(c) by the negative slope of the atomic displacement profile. In Figs. 3(b) and 3(d), the z dependence of the atomic displacements dR_x, dR_y, and dR_z along the x, y, and z directions in the frame of reference of the homogeneous linear displacement is reported. The coefficients A and B obtained from the linear regression of the dr_z spatial profiles reported in Figs. 3(a) and 3(c), are $A = 0.051$ and $B = -0.19$ for the biaxial compression and $A = -0.049$ and $B = -0.22$ for the biaxial expansion. When a biaxial expansion is imposed, the polymeric chain movements benefit from the volume increase. Such a behavior is confirmed by the comparison between Figs. 3(b) and 3(d), where the fluctuations registered in the biaxial expansion test have, on average, a bigger amplitude than in the imposed biaxial compression test. The standard deviation of the atomic displacements spatial profile (its average value is equal to 0) measured in the compression test is 0.015 for dR_x and dR_y, while it is 0.005 for dR_z. In the expansion test, the measured standard deviation of the atomic displacement is 0.020 for dR_x and dR_y, while it amounts to 0.005 for dR_z. The variation of local densities, end to end distances, and backbone orientation angle of the polymeric chains due to the imposed deformation have been calculated; however, no net correlation between these quantities and the atomic displacements shown in Fig. 3 or the Poisson's ratio spatial profile shown in Fig. 4 could be established.

It appears that the statistical fluctuations due to the local material inhomogeneities are too large relative to the perturbations caused by the imposed strain. These observations, in agreement with the small magnitude of the atomic displacement profiles reported in Figs. 3(b) and 3(d), confirm the elastic response of the tested material. As a matter of fact, structural rearrangements within the material would generate a nonelastic deformation of the sample. The local z atomic displacements as a function of the z coordinate induced by the imposed biaxial strain along the x and y axes enable the computation of the variation of the slab dimensions and, therefore, the local Poisson's ratio values.

The locally resolved Poisson's ratio for the PS bulk has been reported in Fig. 4 for an imposed biaxial compression [Fig. 4(a)] and an imposed biaxial expansion [Fig. 4(b)]. The two computer experiments starting from the same initial equilibrated state led to slightly different averages for the Poisson's ratio. As shown in Fig. 4, for the biaxial compression test the average computed Poisson's ratio is equal to 0.44, versus 0.45 for the biaxial expansion test. Experimentally measured [56] and MD based [57,58] Poisson's ratios for PS bulks with different chain lengths are found in a range between 0.34 and 0.38. In analogy to other elastic quantities, the polymer length dependence is rather weak [56–58].

The relaxation time for system reequilibration after the imposed biaxial strain has to be considered in the evaluation of reliable values of the elastic constant. Figure 5 shows that the biaxial compression provides a stable value of 0.44 for the Poisson's ratio after 5–6 ns of reequilibration for the polystyrene bulk. Thereafter, a linear increase of $+0.01$ in

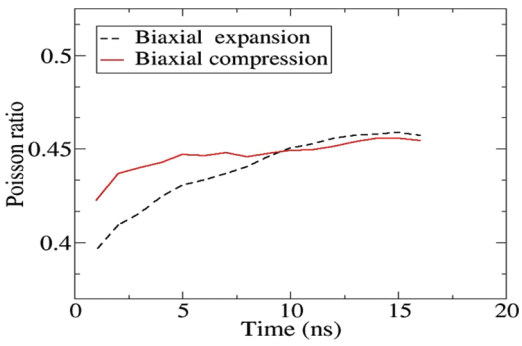

FIG. 5. (Color online) Overall Poisson's ratio of the polystyrene bulk as a function of the allowed relaxation time. The imposed 3% compression/expansion has been applied instantaneously at $t = 0$.

a 10 ns time span has been registered. In the biaxial expansion test, in contrast, the Poisson's ratio value monotonically increases and does not reach a stable value in the period of 15 ns reaching a value of 0.455 at 16 ns.

We can thus conclude that the PS bulk relaxes slightly faster under an imposed compression. This difference can be also deduced from the atomic displacements along the x and y axes (Fig. 3) and the computed Poisson's ratio (Fig. 4). A smaller standard deviation in the Poisson's ratio profile derived in a compression test relative to an expansion test is an advantageous feature in the determination of local mechanical properties. Therefore, the biaxial compression test with a 3% imposed strain will be applied hereafter. The Poisson's ratio values measured for the compression test reported in Fig. 5 show that an acceptable compromise between method accuracy and computational cost can be obtained after 5 ns of relaxation time accepting a 2.5% error in the measured Poisson's ratio.

The statistical fluctuations in an inhomogeneous PS bulk material limit the spatial resolution in local calculations of the Poisson's ratio. A practicable compromise between intended resolution and error bars can be obtained from a set of realizations from independent initial configurations. Therefore, to quantify the accuracy of the here presented approach, the standard deviation of the Poisson's ratio as a function of the averaging volume has been computed.

Figure 6 reports the accessible accuracy in local measurements of the Poisson's ratio as a function of the averaging volume considered. The plot indicates that to compute the elastic quantity locally with a 2.5% variation coefficient, a volume of 2500 nm^3 is required. The required averaging volume can be obtained by averaging a set of equivalent systems generated from uncorrelated initial conditions. With the sample size simulated in the present work, which have an x,y dimension of the simulation box equal to 9.4 and 9.3 nm, a local resolution of 1 nm along the z axis can be obtained from a set of about 30 independent simulations (equivalent to about 4400 PS monomers). The decay of the standard deviation of the Poisson's ratio as a function of the averaging volume has a similar behavior as the function $k * V^{-1/2}$, which mimics the

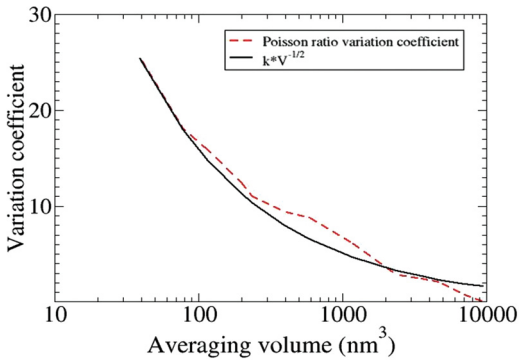

FIG. 6. (Color online) Variation coefficient in % of the Poisson's ratio relative to the bulk value ($\nu = 0.44$) as a function of the averaging volume in a 1 ns time span with a relaxation period of 5 ns, red dashed profile. The black continuous profile reports the function $k * V^{-1/2}$, where k is a fitting constant ($k = 159$), which mimics the decay of the standard deviation for normally distributed uncorrelated samples.

standard deviation decay for normally distributed uncorrelated samples. For volumes above 5000 nm^3 the computed profile deviates significantly in absolute values and in its shape from the spatial profile of the $k * V^{-1/2}$ law. This deviation might be due to the physical constrains in the solid or glassy material in which the molecules or chains have a limited mobility only. In such media, the atomic displacements cannot reach all values prescribed by a normal distribution.

The Poisson's ratio of a silica bulk and silica wafer has also been computed. In an ordered system, such as a crystalline defect-free silica bulk, the local resolution of the mechanical quantities is of minor interest only. Thus, only the average values for the wafer and the silica bulk will be reported here. Imposing a biaxial compression or expansion of 1% to either the silica bulk or the silica wafer, the computed Poisson's ratio is equal to 0.33, with a variation coefficient of 0.1%, which overestimates the values measured in experiments ($\nu = 0.22 \pm 011$) [35,54,59]. Identical values of the computed Poisson's ratio for the bulk and for the silica wafer confirm that the chosen dimensions are sufficient to mimic the mechanical properties of the silica phase. The imposition of a biaxial compression and expansion of 3% enables a structural rearrangement at ambient temperature [60–62]. In the performed simulations, it has been observed that the structure of silica under an imposed 3% strain deviates from the initial α quartz. Such a structural instability results in different computed Poisson's ratios for imposed compressions (0.28, variation coefficient 0.1%,) and expansions (0.37, variation coefficient 0.1%) for the silica bulk and silica wafer.

Once the polystyrene and silica bulk have been studied separately and the influence of the imposed strain on the atomic displacements as well as the Poisson's ratio have been computed, the composite system (c) has been considered. The structural and mechanical properties of the α-quartz silica component are not expected to be modified strongly by the presence of the polystyrene matrix. On the contrary, the soft-matter phase is expected to modify its local properties due to the presence of the interface and, therefore, special emphasis will be directed to the study of the polystyrene phase.

In Fig. 7, the polystyrene mass density profile normalized to the computed bulk mass density of polystyrene, 1033.9 kg/m^3, is plotted. The polystyrene phase spans in the range between $z = 1.15$ nm, and $z = 8.58$ nm, which is the region between the silica wafer and its periodic image. Due to the crystalline

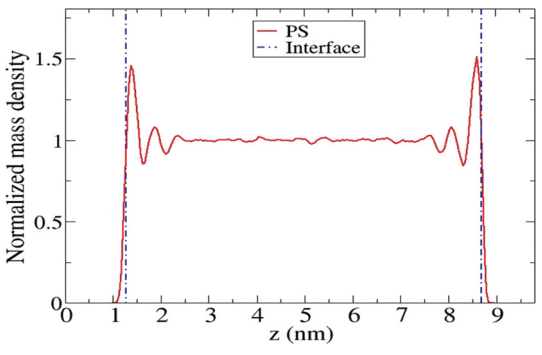

FIG. 7. (Color online) Polystyrene mass density profile, $\rho(z)$, normalized to the polystyrene bulk mass density of 1033.9 kg/m^3, ρ_{bulk}, as a function of the z position.

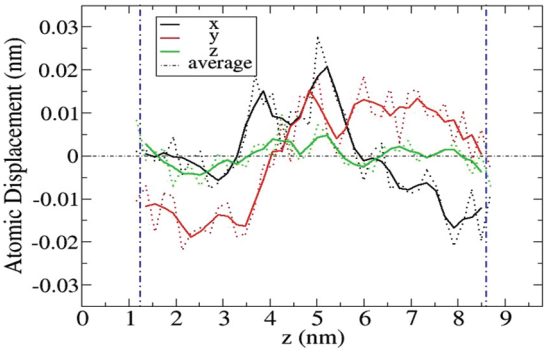

FIG. 8. (Color online) Atomic displacement profiles, dR_x, dR_y, dR_z for the polystyrene-silica composite system under 3% imposed biaxial compression in the frame of reference of the average linear displacement of the PS phase. In the plots, the dotted lines report the local displacement values, while the continuous lines report the five point running average of the displacement profile obtained from a single realization.

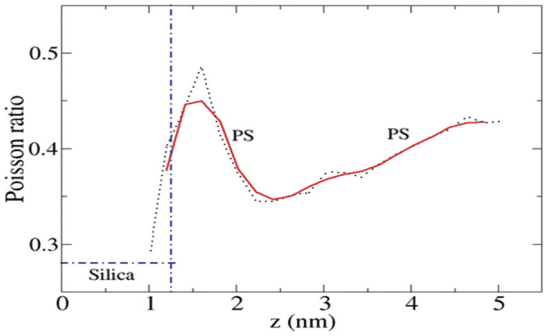

FIG. 9. (Color online) Local Poisson's ratio of the composite system under 3% biaxial compression. In the plot, the dotted line reports the local Poisson's ratio values, while the continuous line reports the five point running average of the Poisson's ratio spatial profile obtained from the average over a set of 30 realizations.

structure of silica, the silica-polystyrene interface is not completely flat. As atomic roughness is present on the surface of the SiO_2 phase, some polystyrene chains can cross the limit defined by the outermost Si atoms, as shown in Fig. 7. At $z = 1.6$ nm and $z = 8.1$ nm, a peak in the concentration profile of the polystyrene monomers has been found, consistent with previous studies of the PS-silica interface [5,46].

In the present work, the fragments of the polystyrene chains that have partially entered the silica phase (shown by the intersection of the PS mass density with the interface in Fig. 7) have not been considered further due to the poor statistics obtainable, which prohibited qualitative and quantitative considerations on the atomic displacements and Poisson's ratio.

To compute the Poisson's ratio spatial profile, the polystyrene-silica composite system (b) has been strained via a 3% biaxial compression along the x and y axes. The obtained spatial z profiles of the induced atomic displacements along the x, y, and z directions have been calculated via Eq. (7), and the derived displacement profiles dR_x, dR_y, and dR_z are reported in Fig. 8.

In Fig. 8 the spatial z profile of the atomic displacement dR_z along the z axis induced by the imposed 3% biaxial compression is reported for the SiO_2-polystyrene composite system. In analogy to the plot in Fig. 3(a), Fig. 8 reports the spatial profile of the atomic displacements, dR_x, dR_y, and dR_z into the x, y, and, z directions for the composite system ($dR_x = dr_x$, $dR_y = dr_y$, and $dR_z = dr_z - (Az - B)$, where $A = 0.052$ and $B = 0.21$). Similar to Fig. 3(b), the spatial dr_z profile does not present sensible fluctuations as a function of the local displacements; therefore only dR_z for the composite system has been reported here. The standard deviations of the atomic displacement profiles in Fig. 8 amount to 0.012 for dR_x and dR_y, while the standard deviation amounts to 0.004 for dR_z. The standard deviations of the atomic displacement profiles are slightly smaller than the ones reported for the PS bulk system of similar system volume and mass. This can be interpreted by the reduced rearrangement capability of the polystyrene chains in the presence of the surface. From a comparison between Fig. 3(a) for the bulk PS system, and Fig. 8 for the PS phase of the composite system, small local collective rearrangements of the polystyrene chains are observed. Among the set of 30 independent realizations performed, a predominant size for the registered collective movement could not be detected for the investigated system type and system size.

In analogy to the procedure adopted for the bulk system, the displacement profiles reported in Fig. 8 can also be used to compute the variation of the slab dimensions and thus the spatial profile of the Poisson's ratio by employing Eq. (11). Since the simulated composite system (b) is symmetrical (two polystyrene-silica interfaces are present), it is possible to improve the statistics of the results by averaging the spatial profile of the Poisson's ratio over the spatial regions near the two sides of the silica wafer. The variation of the Poisson's ratio as a function of the distance from the surface is shown in Fig. 9. It is important to underline here that each slab contains only one phase type while the running average adopted considers the silica and the polystyrene phase independently.

Figure 9 shows the spatial profile of the Poisson's ratio as a function of the z coordinate, which is normal to the silica surface. The silica phase extends between $z = 0$ and $z = 1.25$ nm, while the polystyrene phase starts at $z = 1.10$ nm. As previously mentioned, the computed Poisson's ratio in the range between $z = 1.10$ nm and $z = 1.30$ nm reported in Fig. 9 is affected by an excessively large standard deviation. Thereafter, the Poisson's ratio spatial profile of PS exhibits a maximum of almost 0.5 for $z = 1.6$ nm, which is the limiting value for incompressible liquids. The peak correlates with the first and second mass density maxima reported in Fig. 7. At z positions beyond the fist peak, the Poisson's ratio profile exhibits a minimum at $z = 2.5$ nm (1.4 nm away from the silica phase). Thereafter it increases almost linearly towards the value of 0.42 at $z = 4.5$ nm where it remains almost constant. The measured Poisson's ratio for the bulk system (0.43) is slightly higher than the value measured at 4.5 nm (0.42). This offset is, however, within the error limits of the method and, therefore, the 3.5-nm interval from the surface after which the Poisson's ratio reaches a constant value can be defined as the interphase dimension. We have shown in the present work that the surface has a strong influence on the local values of the Poisson's ratio; therefore the common assumption of a space-independent constant

Poisson's ratio is an oversimplification for micromechanical models which aim to account for interphase effects.

V. CONCLUSIONS AND REMARKS

Mechanical quantities such as the Poisson's ratio are common descriptors of the mechanical behavior of macroscopic systems. The aim of the present work has been to define a method to locally resolve the Poisson's ratio showing the influences of a surface on the spatial profile of the mechanical quantity in a soft-matter phase. Previous MD studies did not show interphase extension beyond 2 nm [5,46,47,50]. From the results reported in Fig. 9, we could deduce an influence of the silica surface covering more than 3.5 nm. Further detailed studies with sufficient statistics, therefore, have to be performed on bigger systems to determine accurately the interphase length dimension after which the Poisson's ratio reaches the bulk value. A detailed description of the soft phase properties under imposed deformation will be presented in forthcoming studies.

A MD based method to compute the local distribution of the Poisson's ratio has been developed based on small-deformation mechanical response. Due to the limitations of PBCs in composite systems in which at least two continuous phases are present, the conventional imposed or induced strain scheme to compute the Poisson's ratio cannot be employed directly. Consequently, a simple generalization of the Poisson's ratio has been derived. A polystyrene bulk, a silica bulk, and a polymer-solid composite material have been characterized under imposed strain and the induced atomic displacements have been reported.

In the polystyrene phase, the employed technique overestimates the Poisson's ratio relative to the available experimental values. This offset can be due to (i) limitations of a force field in the study of mechanical properties. From the results obtained, it seems that the polystyrene chains are not sufficiently stiff enough to correctly predict the mechanical properties of the soft-matter material. This could be due to an offset in the bending and torsional potentials responsible for the tertiary molecular structures. Furthermore, the offset can be due to (ii) system selection, e.g., the polymeric chain length, which for computational limitations has been restricted to 20 monomers. The lack of entanglements within and between polymeric chains leads to polymeric structures that partially differ from experiments and thus to different mechanical properties. Entanglement of polymeric chains can be properly addressed only with larger-scale simulations, e.g., coarse-grained simulations. Finally, the offset can be due to (iii) the assumption of local homogeneity and isotropy. In the silica phase, the performed mechanical analysis allows only the discrimination between *nonauxetic* and *effectively auxetic* [37] materials since the condition of local isotropy does not hold and structural rearrangements have been generated by the imposed strain, whose magnitude has been selected to optimize the interphase description.

To account for the high inhomogeneity of the systems, a detailed study on the magnitude of the fluctuations in the Poisson's ratio spatial profile as a function of the considered volume has been performed. The relationship between the averaging volume and the standard deviation in the computed Poisson's ratio for a polystyrene material has been established, providing the necessary guidelines to investigate similar composite systems.

Despite the observed overestimation of the Poisson's ratio with the presented technique, we have shown that the interphase region between the silica and the polystyrene bulk has a nonlinear Poisson's ratio spatial profile. The extension of the interphase region defined as the length required for the Poisson's ratio to reach the bulk value amounts to approximately 3.5 nm. The local values for the Poisson's ratio have been computed by a method designed with a sufficient generality to be applied to all systems that can be studied via molecular simulations. For consistency and simplicity, the approaches and definitions of the elastic constant used to describe macroscopic systems have been transferred to microscopic systems and the results derived can serve as input to micromechanical modeling.

ACKNOWLEDGMENTS

The present work has been supported by the EU project NanoModel (No. 211778) and by the Deutsche Forschungsgemeinschaft in the Priority Program 1369 "Polymer-Solid Contacts: Interfaces and Interphase." The scientific support of Dr. Denis Davydov (Erlangen) and Dr. Evangelos Voyiatzis (Darmstadt) is gratefully acknowledged.

[1] E. T. Thostenson, C. Li, and T.-W. Chou, Compos. Sci. Technol. **65**, 491 (2005).
[2] S.-Y. Fu, X. Q. Feng, B. Lauke, and Y. W. Mai, Composites, Part B **39**, 933 (2008).
[3] G. Cao, *Nanostructures and Nanomaterials: Synthesis, Properties and Applications* (Imperial College Press, London, 2004).
[4] R. W. Siegel, National Nanotechnology Initiative: Leading to the Next Industrial Revolution, www.nano.gov.
[5] T. V. M. Ndoro, E. Voyiatzis, A. Ghanbari, D. N. Theodorou, M. C. Böhm, and F. Müller-Plathe, Macromolecules **44**, 2316 (2011).
[6] C. Chevigny, N. Jouault, F. Dalmas, F. Boué, and J. Jestin, J. Polym. Sci., Part B: Polym. Phys. **49**, 781 (2011).
[7] N. Sheng, M. C. Boyce, D. M. Parks, G. C. Rutledge, J. I. Abes, and R. E. Cohen, Polymer **2**, 487 (2004).
[8] G. D. Smith, D. Bedrov, L. Li, and O. Byutner, J. Chem. Phys. **117**, 9478 (2002).
[9] D. Brown, P. Mele, S. Marceau, and N. D. Alberola, Macromolecules **36**, 1395 (2003).
[10] D. Brown, S. Marceau, P. Mele, and N. D. Alberola, Macromolecules **41**, 1499 (2008).
[11] L. Yelash, P. Virnau, K. Binder, and W. Paul, Phys. Rev. E **82**, 050801 (2010).
[12] A. A. Gusev and J. J. M. Slot, Adv. Eng. Mater. **3**, 1438 (2001).
[13] A. A. Gusev, J. Mech. Phys. Solids **45**, 1449 (1997).
[14] A. A. Gusev and S. A. Lurie, Macromolecules **42**, 5372 (2009).

[15] S. A. Baeurle, T. Usami, and A. A. Gusev, Polymer **47**, 8604 (2006).
[16] M. Rahimi, H. A. Karimi-Varzaneh, M. C. Böhm, F. Müller-Plathe, S. Pfaller, G. Possart, and P. Steinmann, J. Chem. Phys. **134**, 154108 (2011).
[17] S. Pfaller, G. Possart, P. Steinmann, M. Rahimi, F. Müller-Plathe, and M. C. Böhm, Comput. Mech. **49**, 565 (2011).
[18] G. M. Odegard, T. C. Clancy, and T. S. Gates, Polymers **46**, 553 (2005).
[19] G. M. Odegard, T. S. Gates, L. M. Nicholson, and K. E. Wise, Compos. Sci. Technol. **62**, 1869 (2002).
[20] N. Bakhvalov and G. Panasenko, *Homogenization: Averaging Processes in Periodic Media* (Kluwer Academic Publishers, Dordrecht, 1989).
[21] S. Grigoras, A. A. Gusev, S. Santos, and U. W. Suter, Polymer **43**, 489 (2002).
[22] M. Parrinello and A. Rahman, J. Chem. Phys. **76**, 2662 (1982).
[23] M. Murat and Y. Kantor, Phys. Rev. E **74**, 031124 (2006).
[24] S. Sengupta, P. Niebala, M. Rao, and K. Binder, Phys. Rev. E **61**, 1072 (2000).
[25] M. Parrinello and A. Rahman, Phys. Rev. Lett. **45**, 1196 (1980).
[26] J. R. Ray, Comput. Phys. Rep. **8**, 109 (1988).
[27] K. Yoshimoto, G. J. Papakonstantopoulos, J. F. Lutsko, and J. J. de Pablo, Phys. Rev. B **71**, 184108 (2005).
[28] M. Parrinello and A. Rahman, J. Appl. Phys., **52**, 7182 (1981).
[29] H. J. C. Berendsen, J. P. M. Postma, W. F. van Gunsteren, A. DiNola, and J. R. Haak, J. Chem. Phys. **81**, 3684 (1984).
[30] D. Brown and J. H. R. Clarke, Macromolecules **24**, 2075 (1991).
[31] S. Blonski, W. Brostow, and J. Kubát, Phys. Rev. B **49**, 6494 (1994).
[32] Z. Zhou, J. Chem. Phys. **114**, 8769 (2001).
[33] D. N. Theodorou and U. W. Suter, Macromolecules **18**, 1467 (1985).
[34] D. N. Theodorou and U. W. Suter, Macromolecules **19**, 139 (1986).
[35] G. N. Greaves, A. L. Greer, R. S. Lakes, and T. Rouxel, Nat. Mater. **10**, 823 (2011).
[36] Y. Hundur, R. Hippler, and Z. B. Güvenç, Chin. Phys. Lett. **23**, 1068 (2006).
[37] K. W. Wojciechowski, Comput. Methods Sci. Technol. **11**, 73 (2005).
[38] F. Müller-Plathe, Comput. Phys. Commun. **78**, 77 (1993).
[39] W. L. Jorgensen, D. S. Maxwell, and J. Tirado-Rives, J. Am. Chem. Soc. **118**, 11225 (1996).
[40] F. Müller-Plathe, Macromolecules **29**, 4782 (1996).
[41] H.-J. Qian, P. Carbone, X. Chen, H. A. Karimi-Varzaneh, C. C. Liew, and F. Müller-Plathe, Macromolecules **41**, 9919 (2008).
[42] P. E. M. Lopes, V. Murashov, M. Tazi, E. Demchuk, and A. D. MacKerell, J. Phys. Chem. B **110**, 2782 (2006).
[43] M. P. Allen and D. J. Tildesley, *Computer Simulation of Liquids* (Clarendon Press, Oxford, UK, 1987).
[44] I. G. Tironi, R. Sperb, P. E. Smith, and W. F. van Gunsteren, J. Chem. Phys. **102**, 5451 (1995).
[45] D. R. Lide, *CRC Handbook of Chemistry and Physics*, 74th ed. (CRC Press, Boca Raton, FL1993), Vol. 1.
[46] T. V. M. Ndoro, M. C. Böhm, and F. Müller-Plathe, Macromolecules **45**, 171 (2012).
[47] A. Ghanbari, T. V. M. Ndoro, F. Leroy, M. Rahimi, M. C. Böhm, and F. Müller-Plathe, Macromolecules **45**, 572 (2012).
[48] E. Algaer, M. Alaghemandi, M. C. Böhm, and F. Müller-Plathe, J. Phys. Chem. A **113**, 11487 (2009).
[49] D. Reith, M. Pütz, and F. Müller-Plathe, J. Comput. Chem. **24**, 1624 (2003).
[50] A. Ghanbari, C. M. Böhm, and F. Müller-Plathe, Macromolecules **44**, 5520 (2011).
[51] H. Höcker, G. J. Blake, and P. J. Flory, Trans. Faraday Soc. **67**, 2251 (1971).
[52] R. S. Lakes, Science **235**, 1038 (1987).
[53] R. E. Bolz and G. L. Tuve, *Handbook of Tables for Applied Engineering Science* (The Chemical Rubber Company, Cleveland, OH, 1970), Vol. 124.
[54] W. N. Sharpe Jr., B. Yuan, and R. Vaidyanathan, Micro Electro Mech. Syst. (MEMS) **424**, 1997 (2002 revision).
[55] M. Vacatello, Macromol. Theory Simul. **11**, 757 (2002).
[56] A. V. Lyulin, N. K. Balabaev, M. A. Mazo, and M. A. J. Michels, Macromolecules **37**, 8785 (2004).
[57] J. T. Seitz, J. Appl. Polym. Sci. **49**, 1331 (1993).
[58] T. Raaska, J. S. Niemela, and F. Sundholm, Macromolecules **27**, 5751 (1994).
[59] H. Wahlen and H. Rieger, J. Phys. Soc. Jpn. **69**, 242 (2000).
[60] N. Binggeli, N. R. Keskar, and J. R. Chelikowsky, Phys. Rev. B **49**, 3075 (1994).
[61] J. S. Tse and D. D. Klug, Phys. Rev. Lett. **67**, 3559 (1991).
[62] J. Badro, J. L. Barrat, and P. Gillet, Phys. Rev. Lett. **76**, 772 (1996).